JACS
JOURNAL OF THE AMERICAN CHEMICAL SOCIETY
pubs.acs.org/JACS
Article

Heterometallic Clusters with Multiple Rare Earth Metal−Transition Metal Bonding

Kaiying Shi, Iskander Douair, Genfeng Feng, Penglong Wang, Yue Zhao, Laurent Maron,* and Congqing Zhu*

Cite This: J. Am. Chem. Soc. 2021, 143, 5998−6005
Read Online
ACCESS | Metrics & More | Article Recommendations | Supporting Information

ABSTRACT: Although a series of complexes with rare earth (RE) metal−metal bonds have been reported, complexes which have multiple RE−Rh bonds are unknown. Here we present the identification of the first example of a molecule containing multiple RE−Rh bonds. The complex with multiple Ce−Rh bonds was synthesized by the reduction of a d−f heterometallic molecular cluster Ce{N[$(CH_2CH_2NP^iPr_2)RhCl(COD)]_3$} with excess potassium-graphite. The oxidation state of Ce in **3a** appears to be a mixture of Ce(III) and Ce(IV), which was confirmed by X-ray photoelectron spectroscopy, magnetism, and theoretical investigations (DFT and CASSCF). For comparison, the analogous species with multiple La(III)−Rh and Nd(III)−Rh bonds were also constructed. This study provides a possible route for the construction of complexes with multiple RE metal−metal bonds and an investigation of their potential properties and applications.

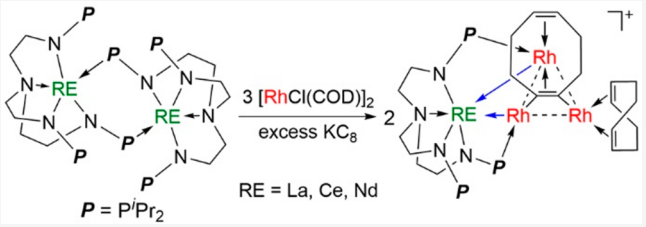

INTRODUCTION

Molecular clusters featuring metal−metal bonds have been fascinating scientists for decades because of their fundamental importance in the understanding of structure and bonding, catalysis, magnetism, and the chemistry of metal surfaces.[1−3] Studies of transition metal (TM)−metal multiple bonds as well as low-valent main-group metal−metal bonds have extended our understanding of chemical bonding, as exemplified by the isolation of complexes with an Re−Re quadruple bond,[4] a Cr−Cr quintuple bond,[5] Zn−Zn and Mg−Mg single bonds,[6,7] and an In_6 molecular chain.[8] Compared with TMs, however, the chemistry of metal−metal bonds involving rare earth (RE) metals is still in its infancy.[9−12]

Since the first RE−TM bond in $(C_5H_5)_2Y(THF)$-$Re_2H_7(PMe_2Ph)_4$ was structurally characterized by Evans and co-workers in 1990,[13] many chemists have studied this important and fundamental field. Representative examples include complexes with RE−Re (RE = Y, La, Sm, Yb, Lu),[14−19] RE−Fe (RE = Nd, Yb, Sc, Y, Lu, La, Dy, Ce),[20−26] Sm−Co,[27] RE−Ni (RE = Sc, Y, La, Lu),[28−31] RE−Pd (RE = Nd, Sc),[32−35] and RE−Pt (RE = Sc, Y, Lu)[36,37] bonds. In addition, some examples with metal−metal bonds between RE and main-group metals have also been reported.[38−48] However, notwithstanding these important discoveries, bimetallic species with a RE−Rh bond are rare[49] and to the best of our knowledge the heterometallic complexes with multiple RE−Rh bonds are unknown.

RE metals in molecular complexes usually exhibit a stable +III oxidation state; the synthesis and characterization of +IV RE species remains a challenge. Cerium, as one of the most abundant RE metals, can adopt a +IV oxidation state in molecular complexes.[50−59] Recently, the +IV oxidation state of RE was extended to Tb and Pr independently by the groups of Mazzanti and La Pierre.[60−64] However, an example of a +IV RE complex with a metal−metal bond has not been reported.

We have recently reported that a multidentate N−P ligand is an effective platform for the construction of heterometallic clusters with multiple actinide metal−transition metal bonds.[65−68] Herein, we report the first example of a complex with multiple Ce−Rh bonds stabilized by this N_4P_3 ligand via a reductive approach starting with chloride-bridged heterometallic clusters containing Ce and Rh. The oxidation state of Ce in this species appears to be a mixture of Ce(III) and Ce(IV). Two similar structures with multiple Nd(III)−Rh and La(III)−Rh bonds were also synthesized for comparison.

RESULTS AND DISCUSSION

Synthesis and Characterization. Treatment of {Ce[N-$(CH_2CH_2NP^iPr_2)_3]\}_2$ (**1a**) with 3 equiv of $[Rh(COD)Cl]_2$ (COD = cyclooctadiene) in tetrahydrofuran (THF) for 2 h at room temperature (RT) afforded a complex Ce{N-$[(CH_2CH_2NP^iPr_2)RhCl(COD)]_3$} (**2a**), which was isolated as a yellow crystalline solid in 85% yield (Scheme 1). The

Received: February 19, 2021
Published: April 7, 2021

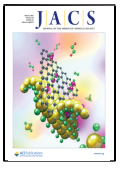

https://doi.org/10.1021/jacs.1c01771
J. Am. Chem. Soc. 2021, 143, 5998−6005

Scheme 1. Synthesis of d−f Heterometallic Molecular Clusters with Multiple RE−TM Bonding

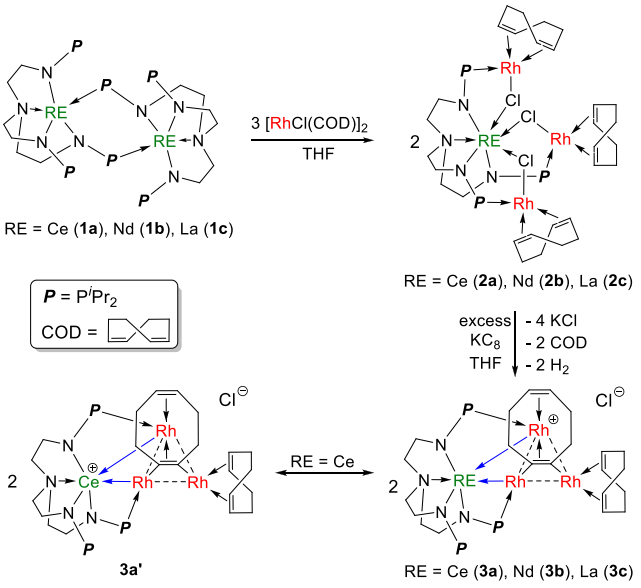

formation of complex **2a** is analogous to the triple FLP-type reactivity previously observed in the reactions of **1a** with a series of organic substrates.[69] A previous study showed that the reduction of the chlorine bridged U−Rh cluster can be used to synthesize species with multiple U−Rh bonds.[66] Accordingly, we examined the reaction of complex **2a** with potassium-graphite (KC_8). A mixture of crystalline **2a** with 2 equiv of KC_8 in THF at RT for 12 h led to the formation of a heterometallic cluster (**3a**) as brown crystals after recrystallization from toluene at −30 °C. Use of excess KC_8 did not alter this result. The detailed mechanism for the formation of complex **3a** is ambiguous but probably involves the reduction of two Rh(I) to Rh(0) atoms by 2 equiv of KC_8 and oxidative addition of two C−H bonds on COD to the Rh(0), and then, reductive elimination of H_2 forms the final product. Analysis of the headspace of this reaction by gas chromatography confirmed the generation of H_2 (Figure S7).

For comparison, the corresponding heterometallic clusters with Nd and La centers were also constructed. The complexes $\{Nd[N(CH_2CH_2NP^iPr_2)_3]\}_2$ (**1b**) and $\{La[N(CH_2CH_2NP^iPr_2)_3]\}_2$ (**1c**) were synthesized by the reaction of $N(CH_2CH_2NHP^iPr_2)_3$ with $Nd[N(SiMe_3)_2]_3$ and $La[N(SiMe_3)_2]_3$ via amine elimination, respectively. Similar to **2a**, complexes $Nd\{N[(CH_2CH_2NP^iPr_2)RhCl(COD)]_3\}$ (**2b**) and $La\{N[(CH_2CH_2NP^iPr_2)RhCl(COD)]_3\}$ (**2c**) were synthesized by the reactions of **1b** and **1c** with 3 equiv of $[RhCl(COD)]_2$ at RT in THF, respectively (Scheme 1). Complexes **2b** and **2c** could react with 2 equiv of KC_8 to generate **3b** and **3c**, respectively, which were isolated as brown crystals in low yields after recrystallization from toluene at −30 °C. Attempts to increase the crystalline yields of complexes **3** by converting the outer sphere Cl^- to PF_6^-, BF_4^-, or BPh_4^- were unsuccessful, and no crystalline products were formed in these processes. Both complexes **2** and **3** are insoluble in aromatic solvents (C_6D_6, C_6D_8), aliphatic hydrocarbons (CD_2Cl_2), ethers (THF-d_8), and even DMSO-d_6, and consequently, their NMR spectra were not obtained.

The solid-state structures of complexes **2a**, **2b**, and **2c** were confirmed by single-crystal X-ray crystallography (Figure 1). The RE metals (Ce, Nd, and La) and three Rh atoms are bridged by three Cl atoms. These complexes exhibit an approximately symmetrical structure with a C_3 axis, Ce1−N1 in **2a**, Nd1−N4 in **2b**, and La1−N1 in **2c**. The RE centers were coordinated with four N atoms from the triamidoamine ligand and three Cl atoms from three [RhCl(COD)] units. The average Rh−P bond lengths of 2.354(2), 2.3442(11), and 2.334(5) Å for **2a**, **2b**, and **2c**, respectively, are similar to the values reported previously.[70] Complex **2b** represents the first example of a heterometallic cluster containing Nd and multiple TMs.

The molecular structures of heterometallic clusters **3a**, **3b**, and **3c** were also confirmed by single-crystal X-ray diffraction (Figure 2). In complex **3a**, the bond length of Ce1−Rh1 (2.8360(4) Å) was slightly shorter than the sum of the covalent radii of Ce and Rh when comparing the interatomic distances (2.88 Å) based on the covalent radii reported by Pyykkö and Atsumi.[71] The Ce1−Rh2 bond length (3.1553(4) Å) was longer than that of Ce1−Rh1 but is almost identical to the length of the only example of a structurally authenticated Ce−TM bond in $(THF)PyCp_2Ce-FeCp(CO)_2$ (3.1546 Å),[21] even though the covalent radius of Rh (1.25 Å) is 0.09 Å larger than that of Fe (1.16 Å). The length of the Rh1−Rh3 (2.6871(4) Å) bond in **3a** is shorter than the Rh1−Rh2 (2.8068(4) Å) and Rh2−Rh3 (2.9345(4) Å) bonds, but all three Rh−Rh bond lengths are obviously longer than the sum of single bond covalent radii for two Rh atoms (2.50 Å), which indicates a weak Rh−Rh interaction between these three Rh atoms.

The bonds in complexes **3b** and **3c** are very similar to those observed in **3a** (Figure 2 and Table 1). The bond length of

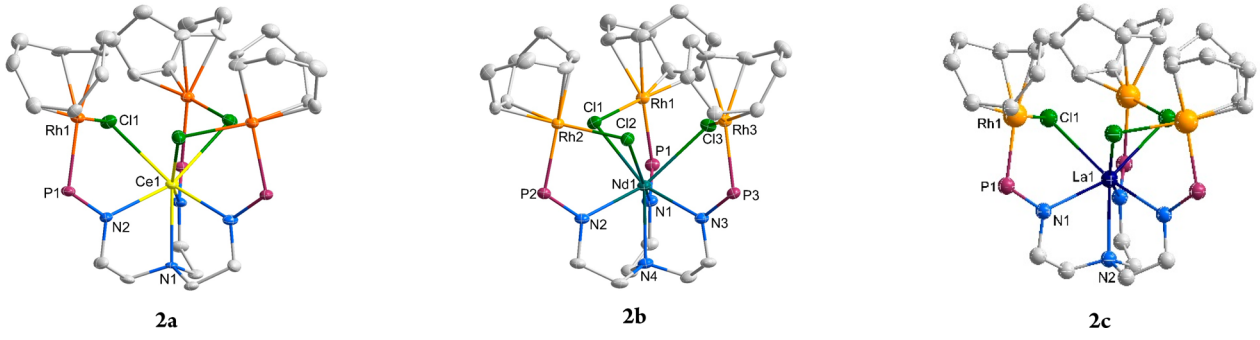

Figure 1. Solid-state structures of **2a**, **2b**, and **2c** obtained by X-ray crystallography with 50% probability ellipsoids. Solvent molecules, hydrogen atoms, and isopropyl moieties in P^iPr_2 are omitted for clarity.

https://doi.org/10.1021/jacs.1c01771
J. Am. Chem. Soc. 2021, 143, 5998−6005

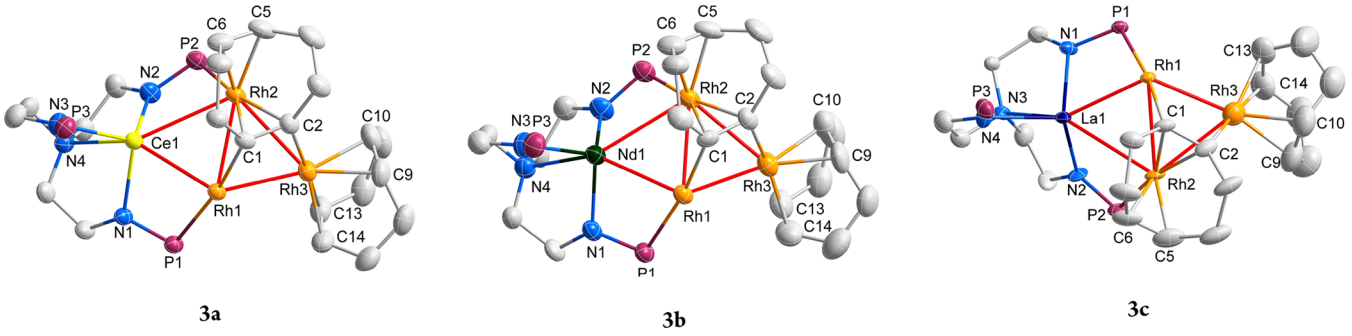

Figure 2. Solid-state structures for cations of **3a**, **3b**, and **3c** obtained by X-ray crystallography with 50% probability ellipsoids. Solvent molecules, hydrogen atoms, and isopropyl moieties in P^iPr_2 are omitted for clarity.

Table 1. Selected Bond Distances (Å) in 3a, 3b, and 3c

	Ln=Ce (**3a**)	Ln=Nd (**3b**)	Ln=La (**3c**)
Ln1–Rh1	2.8360(4)	2.8509(8)	2.8284(10)
Ln1–Rh2	3.1553(4)	3.1438(8)	3.1878(11)
Rh1–Rh2	2.8068(4)	2.8076(9)	2.8179(11)
Rh2–Rh3	2.9345(4)	2.9395(11)	2.8771(16)
Rh1–Rh3	2.6871(4)	2.6908(9)	2.6969(14)
Ln1–N1	2.348(3)	2.299(7)	2.377(9)
Ln1–N2	2.384(3)	2.361(7)	2.417(9)
Ln1–N3	2.380(4)	2.358(7)	2.406(10)
Ln1–N4	2.629(3)	2.590(8)	2.640(10)

Nd1–Rh1 (2.8509(8) Å) is shorter than that of Nd1–Rh2 (3.1438(8) Å) and also shorter than that of the only Nd–Rh bond (2.974 Å) reported previously,[49] which is close to the sum of the interatomic covalent radii of Nd and Rh (2.99 Å).[71] The La1–Rh1 bond length is 2.8284(10) Å in **3c**, which was also shorter than that of La1–Rh2 (3.1878(11) Å). To the best of our knowledge, no structurally characterized species with an La–Rh bond has been reported previously and the La–Rh bond lengths in complex **3c** are close to the previously reported La–Re bond length (3.0721 Å).[17]

The shortest Rh···Cl distances are 3.392 Å in **3a**, 3.928 Å in **3b**, and 4.539 Å in **3c**. These distances are much longer than the Rh–Cl bond lengths in complexes **2** (2.389 Å in **2a**, av. 2.389 Å in **2b**, and 2.428 Å in **2c**) and longer than the sum of single bond covalent radii of Rh and Cl (2.24 Å). Therefore, based on the crystallographic analysis, the Cl ions in complexes **3** are counterbalancing anions in the outer sphere. The Ce1–Rh1 (2.8360(4) Å), Nd1–Rh1 (2.8510(8) Å), and La1–Rh1 (2.8284(10) Å) bonds in heterometallic clusters **3a**, **3b**, and **3c**, respectively, represent the shortest Ce–TM, Nd–TM, and La–TM bonds structurally authenticated by X-ray diffraction.

As shown in Table 1, the average Ce–N_{amido} (2.371(3) Å) and Ce–N_{amine} bond lengths (2.629(3) Å) in **3a** are longer than the Nd–N_{amido} (average of 2.339(7) Å) and Nd–N_{amine} (2.590(8) Å) bond lengths in **3b** and shorter than the bond lengths of La–N_{amido} (average of 2.400(6) Å) and La–N_{amine} (2.640(10) Å) in **3c**, respectively. The differences of the RE–N bond lengths in these complexes are consistent with the order of the Shannon six-coordinate ionic radii for La^{3+} (1.032 Å) > Ce^{3+} (1.01 Å) > Nd^{3+} (0.983 Å). A plot of RE–N distances versus the RE ionic radii was shown in Figure S28, which suggests a trivalent cerium ion in **3a**.

Theoretical Studies. Density functional theory (DFT) calculations were used to determine the nature of the bonding in complexes **2** and **3** and to learn something of the oxidation states of the metals (RE and Rh) in complexes **3a** and **3b**. Geometry optimization without symmetry constraints was first carried out on complexes **2a** and **2b** in order to validate the computational methods (B3PW91), although this method has been well-established since the pioneering work of Maron and Eisenstein.[72] Small core RECPs were used to describe the Ce and Nd centers rather than large core RECPs, that are dedicated to a given oxidation state, even though the +III oxidation state for the RE centers and +I for the Rh ones are evident in complexes **2a** and **2b**. Among others, the Rh–P bond lengths are correctly reproduced by the calculations (2.39 Å vs 2.35 Å experimentally). Unpaired spin densities were determined in both cases (**2a** is a doublet spin state and **2b** a quartet spin state), and both are consistent with a +III oxidation state of Ce and Nd (1.02 for Ce and 3.06 for Nd) and therefore a +I oxidation state of Rh (no unpaired spin density was located on the Rh centers). As mentioned above, these oxidation states were expected for these complexes and can be considered as benchmarks for the computational methods. To further ensure the oxidation states, large core RECPs were used to describe the RE centers and the geometry was fully optimized assuming a +III oxidation state for the RE centers (use of 11e valence electron RECPS as proposed by Maron and Eisenstein in 2000).[72] The optimized geometries using large core RECPs are in good agreement with the results obtained with small core RECPs. For example, the Rh–P bond lengths calculated by the two computational approaches (2.39 Å, see the table in the Theoretical Calculations section of the Supporting Information for a more complete comparison) are identical. A bonding analysis carried out at the natural bonding orbital (NBO) level indicates the presence of 3 center–2 electron (3c–2e) bonds around the RE center, namely, RE–Cl–Rh and RE–N–P, with an ionic character. The latter is highlighted by the RE–Cl and RE–N Wiberg bond indexes (WBI) that are the same for all six interactions and equal to 0.44, in line with ionic–covalent interactions. As expected, the Rh–Cl and Rh–P bonds were found to be more covalent than the RE–Cl and RE–P bonds with WBI values of 0.54 (Rh–Cl) and 0.66 (Rh–P). The covalent contribution in the M–X bonds explains the charges found by the natural population analysis (NPA) where the RE charges are around +1.3 (1.29 for Ce and 1.28 for Nd), whereas the Rh charges are −0.24. The latter may seem surprising for a Rh(I) system but can be explained by the charges of Cl (−0.29), N (−1.2), and P (+1.5) and the covalent contribution in the Rh–X bonds.

Since the computations give correct geometries for the complexes **2a** and **2b** and allow density analysis, calculations were undertaken on the complexes **3a** and **3b** where the RE

https://doi.org/10.1021/jacs.1c01771
J. Am. Chem. Soc. 2021, 143, 5998–6005

and Rh oxidation states are less evident. The optimized geometry of **3b** is in good agreement with the experimental geometry (see the Supporting Information). Among others, the M−M distances are well reproduced (Nd1−Rh1 2.87 vs 2.8510(8) Å, Nd1−Rh2 3.17 vs 3.1433(7) Å, Rh1−Rh2 2.86 vs 2.8077(8) Å, Rh1−Rh3 2.68 vs 2.6908(8) Å, Rh2−Rh3 2.98 vs 2.9398(10) Å). The unpaired spin density (3.16) is located only at the Nd center (Figure 3, top), which is the same as in

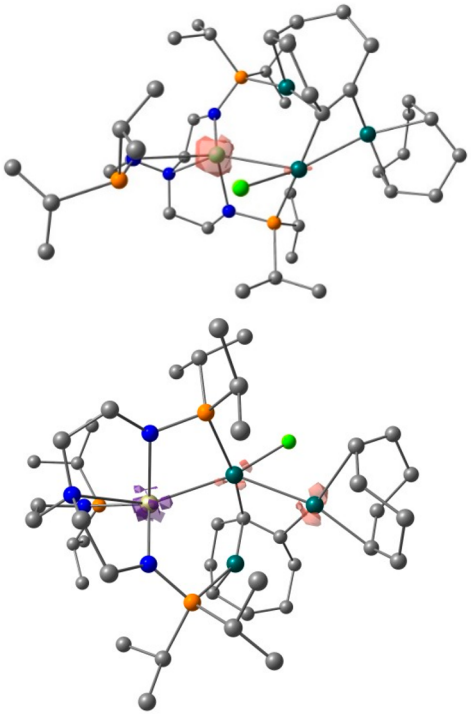

Figure 3. Unpaired spin density plot for the complexes **3b** (top) and **3a** (bottom). Top: The red area around the Nd center indicates unpaired spin density (3.16) accumulation, and it is only located at the RE. Bottom: The red area around the Rh indicates the unpaired spin density accumulation, while the purple contour around the Ce center indicates unpaired spin density depletion.

complex **2b**. Therefore, it can be easily concluded that, quite expectedly, the oxidation state of neodymium is +III, while it is +I for each Rh center in **3b**. NBO calculations indicate the formation of a Nd−Rh bond which is strongly polarized toward Rh (97%) involving a pure d orbital on Rh and a hybride pdf orbital on Nd (23% p, 55% d, and 18% f). The associated WBI is 0.48, which is similar to that of the Nd−Cl bond in complex **2b**. The Rh−Rh interactions are also found at the second-order donor−acceptor NBO level because it involves donation from a filled d orbital on one Rh and an empty d orbital on the other Rh. The associated WBIs are between 0.36 and 0.17.

A similar analysis was carried out on complex **3a**. The optimized geometry of **3a** is in agreement with the experimental one with the M−M distances well reproduced (Ce1−Rh1 2.85 vs 2.8360(4) Å, Ce1−Rh2 3.14 vs 3.1553(4) Å, Rh1−Rh2 2.85 vs 2.8068(4) Å, Rh1−Rh3 2.67 vs 2.6871(4) Å, Rh2−Rh3 2.96 vs 2.9345(4) Å). The unpaired spin density plot (Figure 3, bottom) indicates some spin depletion on Ce and some spin accumulation on Rh. One can therefore conclude that there is a Ce(IV) center present with one Rh(0). To further probe this, large core RECP calculations were carried out assuming either a Ce(III) or a Ce(IV) center. Using a Ce(IV) center, the calculation is a doublet spin state and the unpaired spin density is located at Rh3 (0.84) in line with a Rh(0) and a Ce(IV). Moreover, the bond distances found with the large core RECP associated with Ce(IV) are in better agreement with both the experimental and small core ones than the Ce(III) ones (see the table in the Supporting Information). However, the RE−N bond distances in complex **3a** are found to lie in between the bond distances found for the La(III) and Nd(III) complexes (see Table 1 and the Supporting Information for the computed La values), so that one may conclude that this is compatible with a Ce(III) center in **3a**. In the same way, the computed Ce valence elelectron configuration (see the Supporting Information) is similar to that found for complex **2a**, in line with a Ce(III) center. Therefore, it seems that there is a discrepancy between all analyses (both experimentally and computationally). However, this can be fully understood by analyzing the SOMO of the system (Figure 4). As can be seen, this molecular orbital is fully

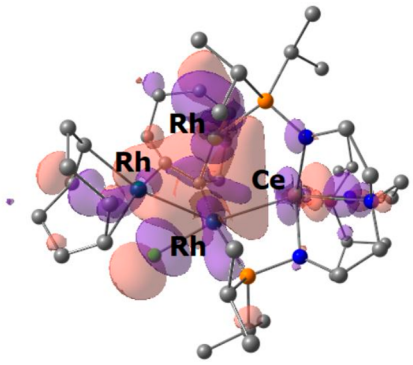

Figure 4. Plot of the SOMO of complex **3a**. The isocontour plot is set to the default (0.03).

delocalized between the Ce and the three Rh centers, with a greater contribution from the three Rh. Therefore, the unpaired electron in the system is delocalized between the four metal centers with a greater probability to be around the three Rh centers rather than being at the Ce. This is thus why a spin depletion is observed at the Ce center and a spin accumulation at the Rh but also why the experimental bond distances are consistent with a +III oxidation state. Therefore, the oxidation state of the Ce center should be in between +III and +IV in **3a**.

It is interesting to note that the SOMO of the Nd(III) complex **3b** and the HOMO of La(III) complex **3c** (Figure 5) does not indicate such electron delocalization of the unpaired electrons from the RE center toward the Rh. This intermediate oxidation state is also in line with the magnetism reported for complex **3a** (see Figure S9). Indeed, the curve of χT vs T is not smooth and is the only one to exhibit a change in slope, indicative to some extent of temperature independent paramagnetism (TIP) and of a multiconfigurational ground state for the Ce complex.[73] To investigate this, CASSCF calculations were carried out on the system. Several active spaces were considered to compute the ground state in order to define the most appropriate one. The small CAS(3,3) was found to be leading to similar results than larger CAS(3,7) or even CAS(7,7), and all are giving a doublet ground state for complex **3a** with a multiconfigurational ground state formed by 68% Ce(III) and 32% Ce(IV). This explains also why the χT

https://doi.org/10.1021/jacs.1c01771
J. Am. Chem. Soc. 2021, 143, 5998−6005

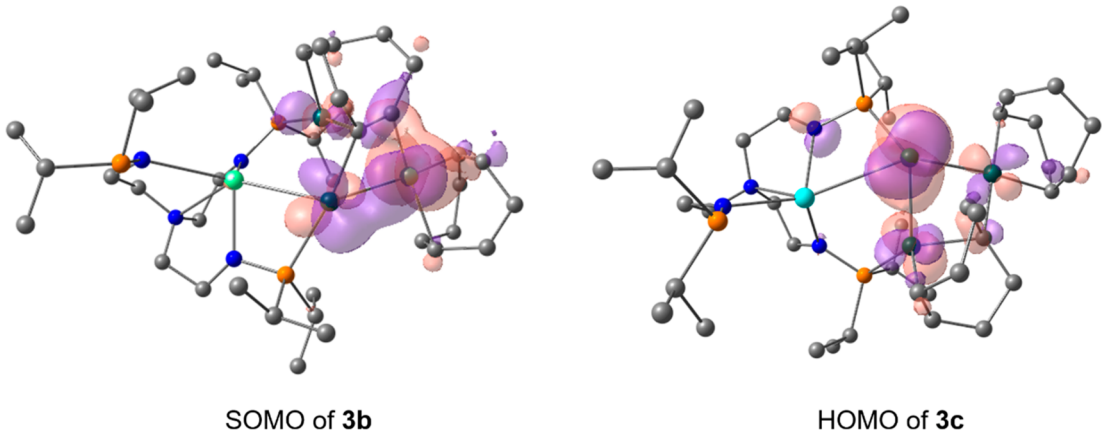

Figure 5. Plot of the highest molecular orbital for **3b** and **3c**. The default isocontour value of 0.03 was used.

vs T plot of **3a** exhibits a slope change, in line with TIP behavior as well as the presence of Ce(IV) fingerprints in XANES experiments. Apart from this important difference in metal center oxidation states, the bonding analysis in **3a** is similar to that in **3b** with a strongly polarized Ce−Rh bond formation and some Rh−Rh bonding interactions (WBI: Ce−Rh 0.51, Rh−Rh 0.40, 0.37, and 0.18).

Magnetic Studies. Variable-temperature magnetic data for clusters **2** and **3** were measured with a superconducting quantum interference device (SQUID) in the solid state. As shown in Figure 6, the magnetic properties of **2b** and **3b** are quite similar, suggesting that they possess the same electronic structure. Except for neodymium, the oxidation state of rhodium is also the same in both complexes. At 300 K, the magnetic moments of **2b** and **3b** are 3.64 μ_B and 3.80 μ_B, respectively, close to the theoretical value (3.62 μ_B) of one Nd(III) ion (f^3, $^4I_{9/2}$, g = 8/11), indicating that Rh(I) is diamagnetic and has a low spin state. Upon cooling, the magnetic moments slowly decreased to 1.55 μ_B and 2.20 μ_B at 1.8 K for **2b** and **3b**, respectively, which is ascribed to the thermal depopulation of Stark levels of Nd(III) ion.

Complexes **2a** and **2b** are isomorphous except for the difference of the lanthanide ion, so **2a** should show the properties of one Ce(III) ion. As expected, the effective moment of **2a** is 2.58 μ_B at 300 K, close to the theoretical value (2.54 μ_B) of Ce(III) ion (f^1, $^2F_{5/2}$, g = 6/7). Similar to **2b**, the moment of **2a** decreases with the cooling due to the orbital contribution and reaches 1.54 μ_B at 1.8 K (Figure 6, bottom). However, complex **3a** exhibits an effective magnetic moment of 2.16 μ_B at 300 K, which is between the theoretical values for a Ce(III) ion (2.54 μ_B) and a Rh(0) ion with S = 1/2 (1.732 μ_B). This result is consistent with the presence of some extent Ce(IV) and Rh(0) components in **3a** (i.e., **3a′** in Scheme 1). The magnetic moment of **3a** slowly decreases to 1.85 μ_B (2 K) with decreasing temperature. Attempts to further oxidize the cerium center in **3a** by $AgBF_4$, $AgBPh_4$, Ph_3CCl, Ph_3CBr, or $PhICl_2$ were unsuccessful, with only some unidentified species being formed. The magnetic moments for lanthanum complexes, **2c** and **3c**, were also measured for comparison. As expected, complex **3c** exhibits a diamagnetic feature in the entire temperature range (Figure S12). However, complex **2c** shows labile $\chi_M T$ values for different samples, and this was attributed to variable amounts of paramagnetic impurities (Figure S12).

X-ray Photoelectron Spectroscopy. The assignments of oxidation states for Nd(III) and Rh(I) in **2b** and **3b** are consistent with the X-ray photoelectron spectroscopy (XPS) data (Figures S13−S16). The Nd-3$d_{5/2}$ and Rh-3$d_{5/2}$ binding energies in **2b** (982.14 and 308.12 eV, respectively) are very close to those found in **3b** (981.53 and 308.60 eV, respectively). The binding energies for Ce-3$d_{3/2}$ (903.41 and 899.70 eV) and Ce-3$d_{5/2}$ (884.86 and 881.36 eV) in **3a** are

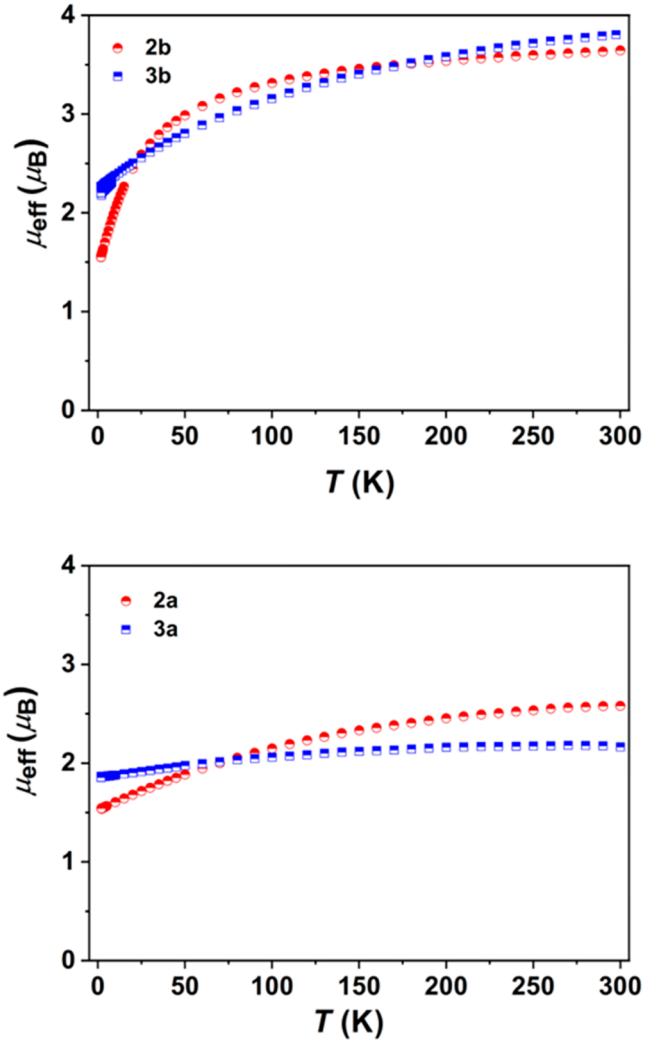

Figure 6. Variable-temperature magnetism for **2b** and **3b** (top) and **2a** and **3a** (bottom).

https://doi.org/10.1021/jacs.1c01771
J. Am. Chem. Soc. 2021, 143, 5998−6005

close to the binding energies for Ce(III) in complex **2a** (903.14 and 898.31 eV for Ce-$3d_{3/2}$; 884.67 and 880.71 eV for Ce-$3d_{5/2}$). The Rh-$3d_{5/2}$ binding energies for **2a** (307.27 eV) and **3a** (307.34 eV) are also close to that of **2b** (308.12 eV). These results indicate the oxidation states of RE and Rh in complexes **2** and **3** are +III and +I, respectively. However, the cerium L_3-edge XANES spectrum of **3a** exhibits two well-separated peaks at about 5732.0 and 5738.6 eV, which are very similar to that found in the reference CeO_2 (Figure S21).[73]

Electronic Absorption Spectra. The UV−vis-NIR electronic absorption spectra for **2** and **3** were recorded in THF at room temperature (Figures S22−S27). Complexes **2a**, **2b**, and **2c** each displayed an intense absorption peak centered around 400 nm and extending over the range of 300−500 nm, and this was tentatively assigned as a ligand to metal charge transfer. In contrast to **2**, the absorption of complexes **3a**, **3b**, and **3c** is very broad, ranging from 300 to 800 nm, and is consistent with their crystalline reddish-brown color.

CONCLUSION

In summary, we report a series of heterometallic clusters containing multiple RE−Rh (RE = La, Ce, and Nd) bonds prepared via a reductive approach. Complexes **3a**, **3b**, and **3c** feature the shortest Ce−TM, Nd−TM, and La−TM bonds authenticated by X-ray diffraction. The oxidation state of Ce in complex **3a** appears to be in between Ce(III) and Ce(IV) and was confirmed by a combined experimental and theoretical study. DFT calculations indicate that the formation of complex **3a** implies the deleocalization of the unpaired electron between the Ce center and the Rh atoms. For complexes **3a**, **3b**, and **3c**, the formation of a RE−Rh bond was detected and involves donation from a filled d orbital on Rh to a pdf hybrid orbital on a RE metal. Our study further confirmed that this N_4P_3 ligand is an effective platform for the construction of d−f heterometallic molecular clusters with multiple RE−TM bonds. Studies on the reactivity of these heterometallic clusters are currently in progress in our laboratory.

ASSOCIATED CONTENT

Supporting Information

The Supporting Information is available free of charge at https://pubs.acs.org/doi/10.1021/jacs.1c01771.

Complete experimental details, NMR and electronic absorption spectrum, SQUID, and computational details including Cartesian coordinates, and crystallographic data (PDF)

Accession Codes

CCDC 2023085−2023089 and 2052118−2052119 contain the supplementary crystallographic data for this paper. These data can be obtained free of charge via www.ccdc.cam.ac.uk/data_request/cif, or by emailing data_request@ccdc.cam.ac.uk, or by contacting The Cambridge Crystallographic Data Centre, 12 Union Road, Cambridge CB2 1EZ, UK; fax: +44 1223 336033.

AUTHOR INFORMATION

Corresponding Authors

Laurent Maron − *LPCNO, CNRS & INSA, Université Paul Sabatier, 31077 Toulouse, France;* orcid.org/0000-0003-2653-8557; Email: laurent.maron@irsamc.ups-tlse.fr

Congqing Zhu − *State Key Laboratory of Coordination Chemistry, Jiangsu Key Laboratory of Advanced Organic Materials, School of Chemistry and Chemical Engineering, Nanjing University, Nanjing 210023, China;* orcid.org/0000-0003-4722-0484; Email: zcq@nju.edu.cn

Authors

Kaiying Shi − *State Key Laboratory of Coordination Chemistry, Jiangsu Key Laboratory of Advanced Organic Materials, School of Chemistry and Chemical Engineering, Nanjing University, Nanjing 210023, China*

Iskander Douair − *LPCNO, CNRS & INSA, Université Paul Sabatier, 31077 Toulouse, France;* orcid.org/0000-0002-7482-5510

Genfeng Feng − *State Key Laboratory of Coordination Chemistry, Jiangsu Key Laboratory of Advanced Organic Materials, School of Chemistry and Chemical Engineering, Nanjing University, Nanjing 210023, China*

Penglong Wang − *State Key Laboratory of Coordination Chemistry, Jiangsu Key Laboratory of Advanced Organic Materials, School of Chemistry and Chemical Engineering, Nanjing University, Nanjing 210023, China*

Yue Zhao − *State Key Laboratory of Coordination Chemistry, Jiangsu Key Laboratory of Advanced Organic Materials, School of Chemistry and Chemical Engineering, Nanjing University, Nanjing 210023, China;* orcid.org/0000-0001-6094-4087

Complete contact information is available at: https://pubs.acs.org/10.1021/jacs.1c01771

Notes

The authors declare no competing financial interest.

ACKNOWLEDGMENTS

This research was supported by the National Natural Science Foundation of China (Grant Nos. 21772088 and 91961116), the Natural Science Foundation of Jiangsu Province (Grant No. BK20200302), the Fundamental Research Funds for the Central Universities (14380216), and Programs for high-level entrepreneurial and innovative talents introduction of Jiangsu Province (group program). The authors thank Prof. You Song at Nanjing University for assistance with magnetic analysis. L.M. is a member of the Institute Universitaire de France. Humboldt Foundation and Chinese Academy of Science are acknowledged for support. CalMip is also gratefully acknowledged for a generous grant of computing time.

REFERENCES

(1) Cotton, F. A., Murillo, C. A., Walton, R. A., Eds. *Multiple Bonds Between Metal Atoms*, 3rd ed; Springer Science and Business Media: New York, 2005; pp 1−796.

(2) Liddle, S. T., Ed. *Molecular Metal-Metal Bonds: Compounds, Synthesis, Properties*; Wiley-VCH: Weinheim, Germany, 2015; pp 1−552.

(3) Wagner, F. R.; Noor, A.; Kempe, R. Ultrashort metal−metal distances and extreme bond orders. *Nat. Chem.* **2009**, *1*, 529−536.

(4) Cotton, F.; Curtis, N.; Harris, C.; Johnson, B.; Lippard, S.; Mague, J.; Robinson, W.; Wood, J. Mononuclear and polynuclear chemistry of rhenium (III): Its pronounced homophilicity. *Science* **1964**, *145*, 1305−1307.

(5) Nguyen, T.; Sutton, A. D.; Brynda, M.; Fettinger, J. C.; Long, G. J.; Power, P. P. Synthesis of a stable compound with fivefold bonding between two chromium(I) centers. *Science* **2005**, *310*, 844−847.

(6) Resa, I.; Carmona, E.; Gutierrez-Puebla, E.; Monge, A. Decamethyldizincocene, a stable compound of Zn(I) with a Zn-Zn bond. *Science* **2004**, *305*, 1136−1138.

(7) Green, S. P.; Jones, C.; Stasch, A. Stable magnesium(I) compounds with Mg-Mg bonds. *Science* **2007**, *318*, 1754−1757.
(8) Hill, M. S.; Hitchcock, P. B.; Pongtavornpinyo, R. A linear homocatenated compound containing six indium centers. *Science* **2006**, *311*, 1904−1907.
(9) Liddle, S. T.; Mills, D. P. Metal−metal bonds in f-element chemistry. *Rev. Dalton Trans.* **2009**, 5592−5605.
(10) Oelkers, B.; Butovskii, M. V.; Kempe, R. f-Element−metal bonding and the use of the bond polarity to build molecular intermetalloids. *Chem. - Eur. J.* **2012**, *18*, 13566−13579.
(11) Patel, D.; Liddle, S. T. f-Element-metal bond chemistry. *Rev. Inorg. Chem.* **2012**, *32*, 1−22.
(12) Butovskii, M. V.; Kempe, R. Rare earth−metal bonding in molecular compounds: Recent advances, challenges, and perspectives. *New J. Chem.* **2015**, *39*, 7544−7558.
(13) Alvarez, D., Jr; Caulton, K. G.; Evans, W. J.; Ziller, J. W. Reversible opening and closing of hetero trimetallic units in $(C_5H_5)_2Y(THF)Re_2H_7(PMe_2Ph)_4$ and $(C_5H_5)_2LuRe_2H_7(PMe_2Ph)_4$. *J. Am. Chem. Soc.* **1990**, *112*, 5674−5676.
(14) Butovskii, M. V.; Tok, O. L.; Wagner, F. R.; Kempe, R. Bismetallocenes: Lanthanoid−transition−metal bonds through alkane elimination. *Angew. Chem., Int. Ed.* **2008**, *47*, 6469−6472.
(15) Butovskii, M. V.; Tok, O. L.; Bezugly, V.; Wagner, F. R.; Kempe, R. Molecular lanthanoid−transition-metal cluster through C−H bond activation by polar metal−metal bonds. *Angew. Chem., Int. Ed.* **2011**, *50*, 7695−7698.
(16) Döring, C.; Dietel, A. M.; Butovskii, M. V.; Bezugly, V.; Wagner, F. R.; Kempe, R. Molecular $[Yb(TM)_2]$ intermetalloids (TM = Ru, Re). *Chem. - Eur. J.* **2010**, *16*, 10679−10683.
(17) Butovskii, M. V.; Döring, C.; Bezugly, V.; Wagner, F. R.; Grin, Y.; Kempe, R. Molecules containing rare-earth atoms solely bonded by transition metals. *Nat. Chem.* **2010**, *2*, 741−744.
(18) Beletskaya, I.; Voskoboynikov, A.; Chuklanova, E.; Kirillova, N.; Shestakova, A.; Parshina, I.; Gusev, A.; Magomedov, G. Bimetallic lanthanide complexes with lanthanide-transition metal bonds. Molecular structure of $(C_4H_8O)(C_5H_5)_2LuRu(CO)_2(C_5H_5)$. The use of ^{139}La NMR spectroscopy. *J. Am. Chem. Soc.* **1993**, *115*, 3156−3166.
(19) Alvarez, D., Jr.; Caulton, K. G.; Evans, W. J.; Ziller, J. W. Synthesis, structure, and reactivity of heterometallic polyhydride complexes of rhenium with yttrium and lutetium. *Inorg. Chem.* **1992**, *31*, 5500−5508.
(20) Burns, C. P.; Yang, X.; Wofford, J. D.; Bhuvanesh, N. S.; Hall, M. B.; Nippe, M. Structure and magnetization dynamics of Dy−Fe and Dy−Ru bonded complexes. *Angew. Chem.* **2018**, *130*, 8276−8280.
(21) Burns, C. P.; Yang, X.; Sung, S.; Wofford, J. D.; Bhuvanesh, N. S.; Hall, M. B.; Nippe, M. Towards understanding of lanthanide−transition metal bonding: Investigations of the first Ce−Fe bonded complex. *Chem. Commun.* **2018**, *54*, 10893−10896.
(22) Diaconescu, P. L. Reactions of aromatic N-heterocycles with d^0f^n-metal alkyl complexes supported by chelating diamide ligands. *Acc. Chem. Res.* **2010**, *43*, 1352−1363.
(23) Deng, H.; Shore, S. G. Direct Yb-Fe interaction in an organometallic "ladder polymer": Synthesis and structure of $\{[(CH_3CN)_3YbFe(CO)_4]_2{\cdot}CH_3CN\}_\infty$. *J. Am. Chem. Soc.* **1991**, *113*, 8538−8540.
(24) Deng, H.; Chun, S.-H.; Florian, P.; Grandinetti, P. J.; Shore, S. G. Direct lanthanide−transition metal interactions: Synthesis of $(NH_3)_2YbFe(CO)_4$ and crystal structures of $\{[(CH_3CN)_3YbFe(CO)_4]_2{\cdot}CH_3CN\}_\infty$ and $[(CH_3CN)_3YbFe(CO)_4]_\infty$. *Inorg. Chem.* **1996**, *35*, 3891−3896.
(25) Blake, M. P.; Kaltsoyannis, N.; Mountford, P. Heterobimetallic complexes containing Ca−Fe or Yb−Fe bonds: Synthesis and molecular and electronic structures of $[M\{CpFe(CO)_2\}_2(THF)_3]_2$ (M = Ca or Yb). *J. Am. Chem. Soc.* **2011**, *133*, 15358−15361.
(26) Arnold, P. L.; McMaster, J.; Liddle, S. T. An unsupported transition metal−lanthanide bond; synthesis and crystal structure of an Nd−Fe amido N-heterocyclic carbene complex. *Chem. Commun.* **2009**, 818−820.
(27) Blake, M. P.; Kaltsoyannis, N.; Mountford, P. Probing the limits of alkaline earth−transition metal bonding: An experimental and computational study. *J. Am. Chem. Soc.* **2015**, *137*, 12352−12368.
(28) Cui, P.; Xiong, C.; Du, J.; Huang, Z.; Xie, S.; Wang, H.; Zhou, S.; Fang, H.; Wang, S. Heterobimetallic scandium−group 10 metal complexes with LM→Sc (LM = Ni, Pd, Pt) dative bonds. *Dalton Trans.* **2020**, *49*, 124−130.
(29) Cui, P.; Huang, X.; Du, J.; Huang, Z. P−C bond cleavage induced Ni(II) complexes bearing rare-earth-metal-based metalloligand and reactivities toward isonitrile, nitrile, and epoxide. *Inorg. Chem.* **2021**, *60*, 3249−3258.
(30) Ramirez, B. L.; Sharma, P.; Eisenhart, R. J.; Gagliardi, L.; Lu, C. C. Bimetallic nickel-lutetium complexes: Tuning the properties and catalytic hydrogenation activity of the Ni site by varying the Lu coordination environment. *Chem. Sci.* **2019**, *10*, 3375−3384.
(31) Ramirez, B. L.; Lu, C. C. Rare-earth supported nickel catalysts for alkyne semihydrogenation: Chemo- and regioselectivity impacted by the Lewis acidity and size of the support. *J. Am. Chem. Soc.* **2020**, *142*, 5396−5407.
(32) Kempe, R.; Noss, H.; Fuhrmann, H. Lanthanide-mediated ligand transfer reactions—A route to late transition metal bisamido complexes. *Chem. - Eur. J.* **2001**, *7*, 1630−1636.
(33) Völcker, F.; Mück, F. M.; Vogiatzis, K. D.; Fink, K.; Roesky, P. W. Bi- and trimetallic rare-earth−palladium complexes ligated by phosphinoamides. *Chem. Commun.* **2015**, *51*, 11761−11764.
(34) Du, J.; Huang, Z.; Zhang, Y.; Wang, S.; Zhou, S.; Fang, H.; Cui, P. A scandium metalloligand-based heterobimetallic Pd−Sc complex: Electronic tuning through a very short Pd→Sc dative bond. *Chem. - Eur. J.* **2019**, *25*, 10149−10155.
(35) Du, J.; Zhang, Y.; Huang, Z.; Zhou, S.; Fang, H.; Cui, P. Heterobimetallic Pd (0) complexes with Pd→Ln (Ln = Sc, Y, Yb, Lu) dative bonds: Rare-earth metal-dominated frustrated Lewis pair-like reactivity. *Dalton Trans.* **2020**, *49*, 12311−12318.
(36) Nakajima, Y.; Hou, Z. Rare-earth-metal/platinum heterobinuclear complexes containing reactive Ln-alkyl groups (Ln = Y, Lu): synthesis, structural characterization, and reactivity. *Organometallics* **2009**, *28*, 6861−6870.
(37) Völcker, F.; Roesky, P. W. Bimetallic rare-earth/platinum complexes ligated by phosphinoamides. *Dalton Trans.* **2016**, *45*, 9429−9435.
(38) Gamer, M. T.; Roesky, P. W.; Konchenko, S. N.; Nava, P.; Ahlrichs, R. Al−Eu and Al−Yb donor−acceptor bonds. *Angew. Chem., Int. Ed.* **2006**, *45*, 4447−4451.
(39) Arnold, P. L.; Liddle, S. T.; McMaster, J.; Jones, C.; Mills, D. P. A lanthanide−gallium complex stabilized by the N-heterocyclic carbene group. *J. Am. Chem. Soc.* **2007**, *129*, 5360−5361.
(40) Wiecko, M.; Roesky, P. W. Gallium (I)−lanthanide (II) donor−acceptor bonds. *Organometallics* **2007**, *26*, 4846−4848.
(41) Minasian, S. G.; Krinsky, J. L.; Rinehart, J. D.; Copping, R.; Tyliszczak, T.; Janousch, M.; Shuh, D. K.; Arnold, J. A comparison of 4f vs 5f metal−metal bonds in $(CpSiMe_3)_3M-ECp^*$(M = Nd, U; E = Al, Ga; $Cp^* = C_5Me_5$): Synthesis, thermodynamics, magnetism, and electronic structure. *J. Am. Chem. Soc.* **2009**, *131*, 13767−13783.
(42) Jones, C.; Stasch, A.; Woodul, W. D. Gallyl lanthanide complexes containing unsupported Ln−Ga (Ln = Sm, Eu, Yb or Tm) bonds. *Chem. Commun.* **2009**, 113−115.
(43) Sanden, T.; Gamer, M. T.; Fagin, A. A.; Chudakova, V. A.; Konchenko, S. N.; Fedushkin, I. L.; Roesky, P. W. Synthesis of unsupported Ln−Ga bonds by salt metathesis and Ga−Ga bond reduction. *Organometallics* **2012**, *31*, 4331−4339.
(44) Schoo, C.; Bestgen, S.; Egeberg, A.; Seibert, J.; Konchenko, S. N.; Feldmann, C.; Roesky, P. W. Samarium polyarsenides derived from nanoscale arsenic. *Angew. Chem., Int. Ed.* **2019**, *58*, 4386−4389.
(45) Zeckert, K.; Zahn, S.; Kirchner, B. Tin−lanthanoid donor−acceptor bonds. *Chem. Commun.* **2010**, *46*, 2638−2640.
(46) Evans, W. J.; Gonzales, S. L.; Ziller, J. W. Organosamarium-mediated synthesis of bismuth-bismuth bonds: x-ray crystal structure

https://doi.org/10.1021/jacs.1c01771
J. Am. Chem. Soc. 2021, 143, 5998−6005

of the first dibismuth complex containing a planar $M_2(\mu\text{-}\eta^2\text{:}\ \eta^2\text{-}Bi_2)$ unit. *J. Am. Chem. Soc.* **1991**, *113*, 9880−9882.
(47) Pugh, T.; Chilton, N. F.; Layfield, R. A. Antimony-ligated dysprosium single-molecule magnets as catalysts for stibine dehydrocoupling. *Chem. Sci.* **2017**, *8*, 2073−2080.
(48) Chen, S.-M.; Xiong, J.; Zhang, Y.-Q.; Ma, F.; Sun, H.-L.; Wang, B.-W.; Gao, S. Dysprosium complexes bearing unsupported Dy^{III}−Ge^{II}/Sn^{II} metal−metal bonds as single-ion magnets. *Chem. Commun.* **2019**, *55*, 8250−8253.
(49) Spannenberg, A.; Oberthür, M.; Noss, H.; Tillack, A.; Arndt, P.; Kempe, R. Metal−metal "communication" of Rh or Pd with Nd in novel heterobinuclear complexes. *Angew. Chem., Int. Ed.* **1998**, *37*, 2079−2082.
(50) Gregson, M.; Lu, E.; McMaster, J.; Lewis, W.; Blake, A. J.; Liddle, S. T. A cerium(IV)−carbon multiple bond. *Angew. Chem., Int. Ed.* **2013**, *52*, 13016−13019.
(51) Gregson, M.; Lu, E.; Mills, D. P.; Tuna, F.; McInnes, E. J.; Hennig, C.; Scheinost, A. C.; McMaster, J.; Lewis, W.; Blake, A. J. The inverse-trans-influence in tetravalent lanthanide and actinide bis-(carbene) complexes. *Nat. Commun.* **2017**, *8*, 14137.
(52) So, Y. M.; Wang, G. C.; Li, Y.; Sung, H. H. Y.; Williams, I. D.; Lin, Z.; Leung, W. H. A tetravalent cerium complex containing a Ce=O bond. *Angew. Chem.* **2014**, *126*, 1652−1655.
(53) Damon, P. L.; Wu, G.; Kaltsoyannis, N.; Hayton, T. W. Formation of a Ce(IV) oxo complex via inner sphere nitrate reduction. *J. Am. Chem. Soc.* **2016**, *138*, 12743−12746.
(54) So, Y.-M.; Li, Y.; Au-Yeung, K.-C.; Wang, G.-C.; Wong, K.-L.; Sung, H. H.; Arnold, P. L.; Williams, I. D.; Lin, Z.; Leung, W.-H. Probing the reactivity of the Ce=O multiple bond in a cerium (IV) oxo complex. *Inorg. Chem.* **2016**, *55*, 10003−10012.
(55) Assefa, M. K.; Wu, G.; Hayton, T. W. Synthesis of a terminal Ce(IV) oxo complex by photolysis of a Ce(III) nitrate complex. *Chem. Sci.* **2017**, *8*, 7873−7878.
(56) Solola, L. A.; Zabula, A. V.; Dorfner, W. L.; Manor, B. C.; Carroll, P. J.; Schelter, E. J. An alkali metal-capped cerium(IV) imido complex. *J. Am. Chem. Soc.* **2016**, *138*, 6928−6931.
(57) Solola, L. A.; Zabula, A. V.; Dorfner, W. L.; Manor, B. C.; Carroll, P. J.; Schelter, E. J. Cerium(IV) imido complexes: Structural, computational, and reactivity studies. *J. Am. Chem. Soc.* **2017**, *139*, 2435−2442.
(58) Rice, N. T.; Su, J.; Gompa, T. P.; Russo, D. R.; Telser, J.; Palatinus, L.; Bacsa, J.; Yang, P.; Batista, E. R.; La Pierre, H. S. Homoleptic imidophosphorane stabilization of tetravalent cerium. *Inorg. Chem.* **2019**, *58*, 5289−5304.
(59) Cheisson, T.; Kersey, K. D.; Mahieu, N.; McSkimming, A.; Gau, M. R.; Carroll, P. J.; Schelter, E. J. Multiple bonding in lanthanides and actinides: Direct comparison of covalency in thorium(IV)-and cerium(IV)-imido complexes. *J. Am. Chem. Soc.* **2019**, *141*, 9185−9190.
(60) Palumbo, C. T.; Zivkovic, I.; Scopelliti, R.; Mazzanti, M. Molecular complex of Tb in the + 4 oxidation state. *J. Am. Chem. Soc.* **2019**, *141*, 9827−9831.
(61) Willauer, A. R.; Palumbo, C. T.; Scopelliti, R.; Zivkovic, I.; Douair, I.; Maron, L.; Mazzanti, M. Stabilization of the oxidation state +IV in siloxide-supported terbium compounds. *Angew. Chem.* **2020**, *132*, 3577−3581.
(62) Rice, N. T.; Popov, I. A.; Russo, D. R.; Bacsa, J.; Batista, E. R.; Yang, P.; Telser, J.; La Pierre, H. S. Design, isolation, and spectroscopic analysis of a tetravalent terbium complex. *J. Am. Chem. Soc.* **2019**, *141*, 13222−13233.
(63) Willauer, A. R.; Palumbo, C. T.; Fadaei-Tirani, F.; Zivkovic, I.; Douair, I.; Maron, L.; Mazzanti, M. Accessing the +IV oxidation state in molecular complexes of praseodymium. *J. Am. Chem. Soc.* **2020**, *142*, 5538−5542.
(64) Rice, N. T.; Popov, I. A.; Russo, D. R.; Gompa, T. P.; Ramanathan, A.; Bacsa, J.; Batista, E. R.; Yang, P.; La Pierre, H. S. Comparison of tetravalent cerium and terbium ions in a conserved, homoleptic imidophosphorane ligand field. *Chem. Sci.* **2020**, *11*, 6149−6159.
(65) Feng, G.; Zhang, M.; Shao, D.; Wang, X.; Wang, S.; Maron, L.; Zhu, C. Transition-metal-bridged bimetallic clusters with multiple uranium−metal bonds. *Nat. Chem.* **2019**, *11*, 248−253.
(66) Feng, G.; Zhang, M.; Wang, P.; Wang, S.; Maron, L.; Zhu, C. Identification of a uranium−rhodium triple bond in a heterometallic cluster. *Proc. Natl. Acad. Sci. U. S. A.* **2019**, *116*, 17654−17658.
(67) Xin, X.; Douair, I.; Zhao, Y.; Wang, S.; Maron, L.; Zhu, C. Dinitrogen cleavage by a heterometallic cluster featuring multiple uranium−rhodium bonds. *J. Am. Chem. Soc.* **2020**, *142*, 15004−15011.
(68) Feng, G.; McCabe, K. N.; Wang, S.; Maron, L.; Zhu, C. Construction of heterometallic clusters with multiple uranium−metal bonds by using dianionic nitrogen−phosphorus ligands. *Chem. Sci.* **2020**, *11*, 7585−7592.
(69) Sun, X.; Su, W.; Shi, K.; Xie, Z.; Zhu, C. Triple frustrated Lewis pair-type reactivity on a single rare earth metal center. *Chem. - Eur. J.* **2020**, *26*, 5354−5359.
(70) Xin, X.; Zhu, C. Isolation of heterometallic cerium(III) complexes with a multidentate nitrogen−phosphorus ligand. *Dalton Trans.* **2020**, *49*, 603−607.
(71) Pyykkö, P.; Atsumi, M. Molecular single-bond covalent radii for elements 1−118. *Chem. - Eur. J.* **2009**, *15*, 186−197.
(72) Maron, L.; Eisenstein, O. Do f electrons play a role in the lanthanide-ligands bonds. A DFT study on $Ln(NR_2)_3$ with R = H, SiH_3. *J. Phys. Chem. A* **2000**, *104*, 7140−7143.
(73) Halbach, R. L.; Nocton, G.; Booth, C. H.; Maron, L.; Andersen, R. A. Cerium tetrakis(tropolonate) and cerium tetrakis-(acetylacetonate) are not diamagnetic but temperature-independent paramagnets. *Inorg. Chem.* **2018**, *57*, 7290−7298.

https://doi.org/10.1021/jacs.1c01771
J. Am. Chem. Soc. 2021, 143, 5998−6005